Summation of supraharmonic currents (2–150 kHz) from EV fast charging stations

Electric Power Systems Research 220 (2023) 109371

Contents lists available at ScienceDirect

Electric Power Systems Research

journal homepage: www.elsevier.com/locate/epsr

Summation of supraharmonic currents (2–150 kHz) from EV fast charging stations☆

Tim Slangen *[,1], Vladimir Ćuk[1], Sjef Cobben[1]

Eindhoven University of Technology, PO Box 513, 5600MB, Eindhoven, The Netherlands

ARTICLE INFO

Keywords:
Supraharmonics
Summation
Fast-charging station
High-frequency distortion
Diversity factor
Electric vehicle charging

ABSTRACT

This paper presents the outcomes of a study of the summation of supraharmonic (SH) currents from electric vehicle fast-charging stations (FCS), based on a field measurement in an installation with four 350 kW FCSs. FCSs can contribute to SH emission, between 2 and 150 kHz, in the network and their impact on the grid is quantified by the summation of SH components. Little is known about the summation of SHs in an installation with a power of hundreds of kW, therefore this article aims to contribute to the understanding of the SH current emission and their summation in practice. The results show that the total SH current from the installation increases with the number of active chargers, but not monotonous and that the emission is not constant over time. A diversity factor is proposed and the relation between total and summed current is analyzed to provide further insight into the role of absorption by other chargers. The findings are a step towards modeling the SH summation for FCSs and other installations with large power-electronic devices.

1. Introduction

With the growing concerns about climate change, the transition from fossil- to electric mobility is accelerating. Electric vehicles (EVs) have the potential to be supplied with renewable electricity, significantly reducing greenhouse gas emissions and fossil fuel usage. To charge an electric vehicle, there are presently 2 widely adopted options; slow charging with the onboard charger (OBC) of the EV itself – mostly limited to 22 kW – and fast charging (FC) with charging power between 50 kW and 350 kW which are expected to increase. Whereas slow charging is convenient for charging overnight at home or during daytime at the office (4–8 h), FC has the advantage of adding a large amount of range (e.g. 200 km) in a short amount of time (e.g. 15 min). The latter is especially of interest when traveling long distances or for applications in public transport and for trucks where often is limited time to charge the large batteries during several hours using slow charging. To improve the air quality in cities, full electric public transport solutions can replace the air-polluting diesel and gasoline vehicles. To achieve this, a comprehensive FC infrastructure is needed both within highly populated residential areas and in more remote highway locations. Fast charging stations (FCSs) have a high power demand compared to slow charging and there is limited flexibility for algorithms like smart charging because the charging sessions are very short compared to charging using the OBC. Furthermore, FCSs are generally installed in groups of two or more, offering different charging power. Most public FC locations in The Netherlands consist of one or more relatively small 50 kW chargers and are the last years extended with multiple 150 kW or 350 kW chargers. High charge power is needed to fulfill the demand of charging the battery of an EV from 20 to 80 percent in approximately 15 min [1].

1.1. Literature review

The grid impact of FCSs is still under investigation. FCSs require a strong dedicated grid connection to accommodate the high peak power demand. Next to the high power demand, FCSs can affect the power quality of the grid and may interact with each other. For instance, FCSs can be a source of harmonics and supraharmonics (SHs) [1–3]. SHs are voltage and current distortions with a frequency between 2 and 150 kHz and can be present in LV- [4–7], MV- [8] and HV-grids [9]. The phenomenon has gained more attention, especially in the last decade, due to the increasing number of self-commutated converters that lead to more SH disturbances, outside the classical range (below 2 or 2.5 kHz) for power quality [10]. The first reports describing issues related to SHs refer to them as high-order harmonics or oscillations in the kHz range. The issues reported include failing cable terminations in a converter-based installation [11], malfunction or damage of office

☆ This research is part of the project TEPQEV and supported by Topsector Energy-subsidy of the Dutch Ministry of Economic Affairs and Climate.
* Corresponding author.
E-mail addresses: t.m.h.slangen@tue.nl (T. Slangen), v.cuk@tue.nl (V. Ćuk), j.f.g.cobben@tue.nl (S. Cobben).
[1] The authors are with the Electrical Energy Systems group at Eindhoven University of Technology.

https://doi.org/10.1016/j.epsr.2023.109371
Received 13 December 2022; Received in revised form 16 February 2023; Accepted 26 March 2023

equipment, and excessive audible noise [12]. Presently, it is known that SHs can result in several unwanted effects to and interference with devices, network components, and power line communication. Recently, various reports about this have been presented in [4].

Regarding the summation of supraharmonic currents, in [13] it was found for LEDs that for an increasing number of devices, the SH grid current does not increase proportionally with the number of devices, rather, the increase slows down as the emission mainly flows between neighboring devices. This behavior is further detailed in [14] and a summation law is described. Recently, in [15] different summation models are experimentally tested on an installation with LED lighting and a new summation law is proposed based on the ratio between device- and grid capacitance. It is shown that the emission from an installation at a certain point decreases for an increasing number of devices. It is one of the objectives of the current research to see if the same findings apply to other types of converters with a much larger power, like in FCSs.

Measuring the SH current (emission) from a device can be challenging in situations where other devices emitting SHs are present, as they can cause additional SH emissions from the device to be emitted. This apparent emission from the device under test (primary device) which originates from another (secondary) device in the grid is first defined in [14] as secondary emission and the difference is further detailed in [16]. To assess the primary emission of a device, a sinusoidal background voltage without harmonic and SH distortion is required, which is unachievable in most field measurements.

The emission of harmonic currents from FCSs in low voltage (LV) networks is studied in [17] and it is concluded that the emissions mostly remain within the limits for full-power operation. The same is concluded in [3] for an installation in The Netherlands and in [2] for several installations in Germany and China. For installations, this is mainly due to the diversity of phase angles that can cause the cancellation of the individual harmonics from the FCSs.

For OBCs the emissions are determined in [18–20] and it is concluded that OBCs can contribute to harmonics and supraharmonic emissions in the grid. Component-based models describing the harmonic grid impact of OBCs in the time-domain have been presented in [21–23] but do not include SH emissions.

Modeling the harmonic emission of FCSs is performed in [24] for a relatively small FCS using a fingerprint-based Norton approach, in [25] for larger FCSs using an advanced converter harmonic model based on a case study and in [26] using time-domain simulations.

Several methods exist to reduce the harmonic distortions from a device. For instance, by using advanced control methods for the power factor correction circuit [27] or by selective harmonic elimination [28] the overall harmonic distortion can be effectively reduced. For SHs, however, such methods do not exist yet.

The focus of this research is on an installation with FCSs in an LV system, connected to the MV grid through a distribution transformer. Based on experiments by [29] it is expected that the transfer of SH emissions upstream (from LV to MV) is generally damped, minimizing the effect on the MV grid. Future installations with higher total power are under development and can be connected directly to the MV grid. In that case, the impedance of the upstream system is different [30] and the total current is lower, and it is unknown what the SH emission of such an installation is.

1.2. Paper contributions and structure

To assess the grid impact of FCSs in terms of supraharmonic distortion and to understand the summation of SH components in practice, knowledge of the emission from both individual devices and installations with multiple devices is required. In this research, a comprehensive study on the SH emission and summation from FCSs is presented, based on measurements in an installation with 4 FCSs of 350 kW. The emission from the installation and individual chargers is observed during a week for a variable number of chargers active. The summation of SH components is further studied and the relation between the total measured current and the arithmetical sum of individual currents is described using a diversity factor for supraharmonics. The objectives of this research are to study, for a different number of active chargers:

- The SH emission of a single FCS.
- The summation of SH currents in the installation.
- The relation between individual charger currents and total current.
- The factors influencing the summation.

In Section 2 the methodology is discussed. Section 3 presents an analysis of the measurement results regarding SH emission from individual chargers and the summation for the installation is studied in Section 4. The diversity factor for supraharmonics is presented in Section 5 and applied to the results. A discussion of the results is provided in Section 6 and the most important conclusions and recommendations for further research are found in Section 7.

Table 1
Charger specifications.

DC output voltage range (V)	460–800
Max DC output current (A)	700
Max DC output power (kW)	350
Topology	2-level AFE
Switching frequency	3.6 kHz
Peak efficiency	96%
Power factor (>50% loading)	0.99

2. Methodology

2.1. Measurement location

The network topology is as presented in Fig. 1, with a 10 kV/0.4 kV distribution transformer rated 1600 kVA and $U_k = 6.1\%$ (percentage impedance). Based on the full- and no-load losses of the transformer, the U_k value, and the rated power, the X/R ratio is calculated, $X/R = 7.9$. Connected to the transformer are 4 FCSs rated 350 kW with specifications as shown in Table 1. No other loads are connected to this transformer. The measurement points are as indicated at the conductors of individual FCSs (I_i) and the transformer feeder (I_{tot}). Voltage is measured at the busbar for all 3 phases between line and neutral. The location is a public transport bus depot where next to this network, 2 other transformers with multiple 50 and 350 kW chargers are installed. Because this transformer has the highest expected loading and is a homogeneous installation, it is selected for the measurements. Cable types and length as in the figure, all FCSs are connected using the same cables with approximately the same length. The measured active power of the chargers is mostly 300 kW throughout the day and 50 kW during the night, when the chargers are used for slower charging. This did however not result in a change in emission.

2.2. Measurement equipment

The measurement device is a Yokogawa DL350 mobile oscilloscope. The device has 8 channels with a maximum sample rate of 1 MS/s, 16-bit resolution, and 300 kHz bandwidth. The voltage is measured using 10:1 probes and the current using PEM LFR 03/3 current probes with a sensitivity of 10 mV/A, and a bandwidth of 600 kHz (−3 dB). The noise floor for the 2–150 kHz range is determined based on the measurements and is at maximum 100 mA. The resolution of the measurements is obtained by the ratio between the maximum input voltage of the scope (60 V) and the 16-bit resolution, resulting in a resolution of 9.2 mV for the voltage- and 92 mA for the current. It is assumed the scope does not introduce bias errors, and the only uncertainty introduced is due to the quantization error, which is 4.6 mV for the voltage and 46 mA for

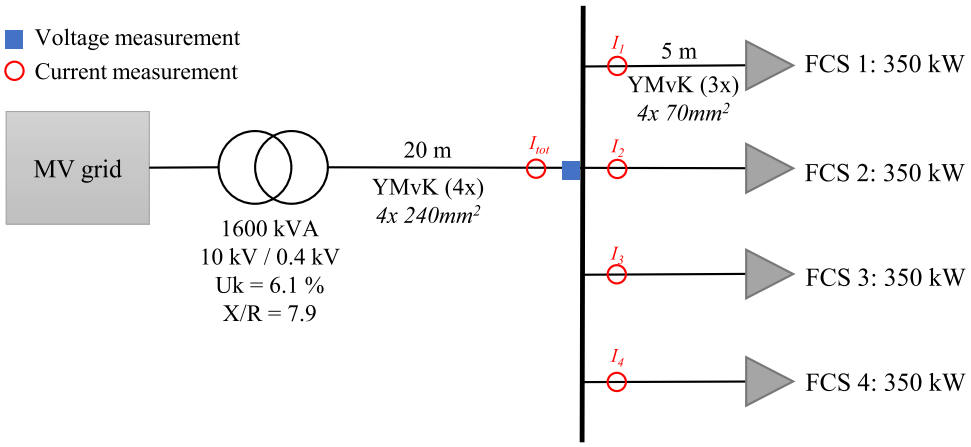

Fig. 1. Network topology at the measurement site. Voltage measurement at the LV busbar in the distribution cabinet, about 20 m from the MV/LV transformer. Current measurement at all outgoing feeders (I_i) and the transformer connection (I_{tot}).

the current. Measurements are conducted during a week (one snapshot per 5 min), with a sample duration of 500 ms, and a sample rate of 1 MS/s.

2.3. Analysis of supraharmonic emission

The individual frequency components of the voltage and current are calculated using the Fast Fourier Transform (FFT) function of MATLAB for the first 200 ms of the 500 ms sample, yielding 100.000 components in the single-sided spectrum with a resolution of 5 Hz. The frequency components are denoted as I_f where f is the center frequency of the 5 Hz frequency component. There is no normative method yet to analyze SH components, only informative methods as per the IEC standards [31,32]. The authors of [10,33] present a comparison of, among others, the proposed IEC methods for the measurement and analysis of supraharmonic components.

In this research, the assessment of supraharmonic components is performed by aggregating the I_f values in supraharmonic bins (I_{sh}) using the root sum square (RSS) as

$$I_{sh} = \sqrt{\sum_{f=f_{min}}^{f_{max}} I_f^2} \tag{1}$$

with f_{min} is the lower frequency border of the bin and f_{max} the upper frequency border of the bin. Similarly, V_{sh} is calculated. The bin frequencies are selected based on the highest emission frequencies. Alternatively, I_{sh} can be denoted as SHC (supraharmonic current), which is obtained using the same expression. The total SH current (TSHC) is obtained when considering I_{sh} for the complete range from 2 to 150 kHz, but in this research I_{sh} is used to isolate smaller bins with emission to improve the clarity when comparing different components.

2.4. Data classification

For the analysis of the impact of a single- or multiple chargers active, the data is classified. Based on the measurements, the minimal charging current is about 43 A at the AC side. For this reason, a threshold of 20 A is used to classify the on/off state of the charger. In this way, for each measurement, the state of the charger is determined, and the total number of active chargers (N) is calculated.

3. Results on emission

3.1. Primary SH emission

In Fig. 2 the voltage and total current waveforms for a measurement with 3 FCSs active is presented. For both the voltage and the current a high-frequency component is visible, in this case with a frequency of approximately 7.0 kHz. The frequency bands with the highest SH emission for one FCS is presented in Fig. 3, obtained using a 200 ms measurement window. The harmonic emission is also shown. Ideally, the characterization of the emission from a device is achieved in a lab environment without influence from background distortion. In this research, the influence of other chargers is eliminated by analyzing the moments when other chargers are turned off. However, the spectra might contain background distortion from other devices that are not monitored (e.g. peripheral equipment) in the same installation or the upstream MV network. However, an analysis of this background distortion with all chargers disconnected pointed out that the background emission frequencies are not coinciding with the SH emission from the chargers, and that the amplitudes are much lower than the emission from the chargers.

For the chargers, the highest emission components (>100 mA) are observed between 3.0 and 4.0 kHz and between 6.7 and 7.7 kHz, these are the bins of interest with a bandwidth of 1 kHz. The emission frequencies of the first bin align with the switching frequency of the charger according to the specifications (3.6 kHz). Multiple peaks are observed that are 100 Hz (two times the fundamental frequency) apart. These properties are a characteristic of active front-end devices using pulse-width modulation (PWM), such as described in [34].

3.2. Secondary SH emission, for 2 devices

Next to the primary emission, the FCSs might absorb SH emission from other FCSs, resulting in secondary emission. In this research, it is of interest to see whether chargers that are not active still absorb emission from the installation, resulting in secondary emission from the secondary device, without the presence of primary emission. To study this, the data points where chargers 3 and 4 (FCS-3 and FCS-4) are never active are selected, thus focusing only on chargers 1 and 2 (FCS-1 and FCS-2). Then, the data points are classified into 4 groups, both chargers 1 and 2 active, only charger 1 active, only charger 2 active, and none of the chargers active. The measured SH emission is presented in Fig. 4. It is observed that when one of the chargers is active and emits emission, there is no SH emission measured at the other charger. This means that when the chargers are inactive the charger does not contribute to the absorption of the emission. Hence, all emissions will flow towards the grid. This is either due to their filters disconnecting from the grid when turned off, or they block the secondary emission effectively. When both chargers are active, the emission is seen for both of them but with the amplitude in a band, meaning that secondary emission is absorbed mutually and this implies that the filters disconnect when the chargers are turned off. Also, as the

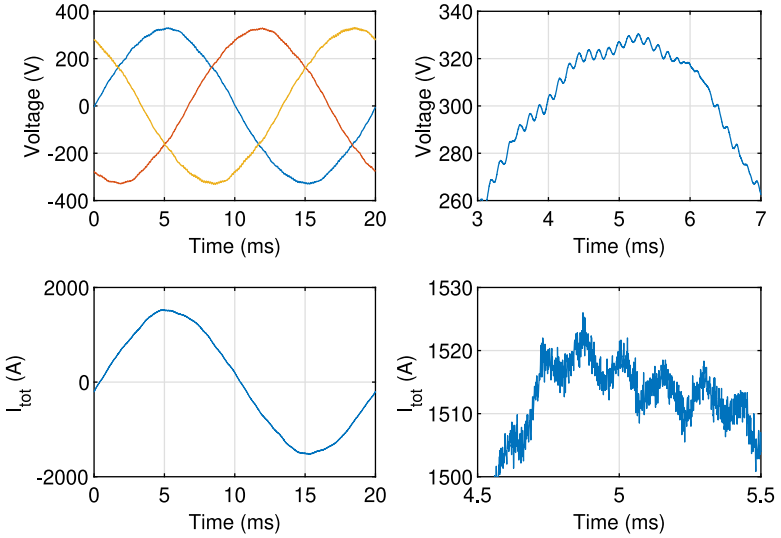

Fig. 2. Voltage and total current (I_{tot}) waveforms from a measurement with 3 chargers active. A high-frequency oscillation with a period of ≈0.14 ms (≈7.0 kHz) is visible. In the right figures, a zoomed part of the left figures is presented for more detail.

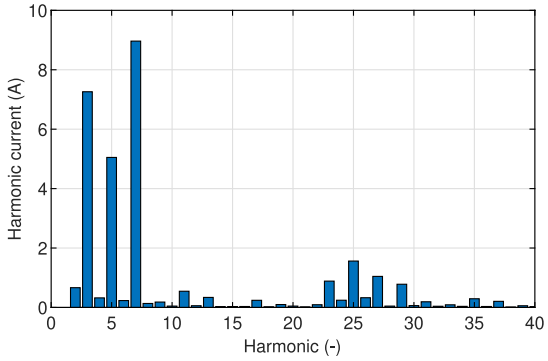

(a) Harmonic current spectrum.

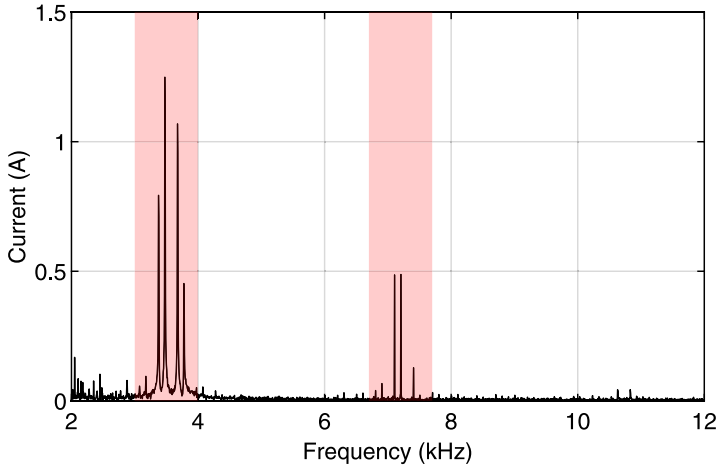

(b) SH emission spectrum between 2 and 12 kHz, obtained using a 200 ms measurement window. Bins of interest are 3.0-4.0 kHz and 6.7-7.7 kHz (marked).

Fig. 3. Harmonic (a) and supraharmonic (b) spectra for FCS 1.

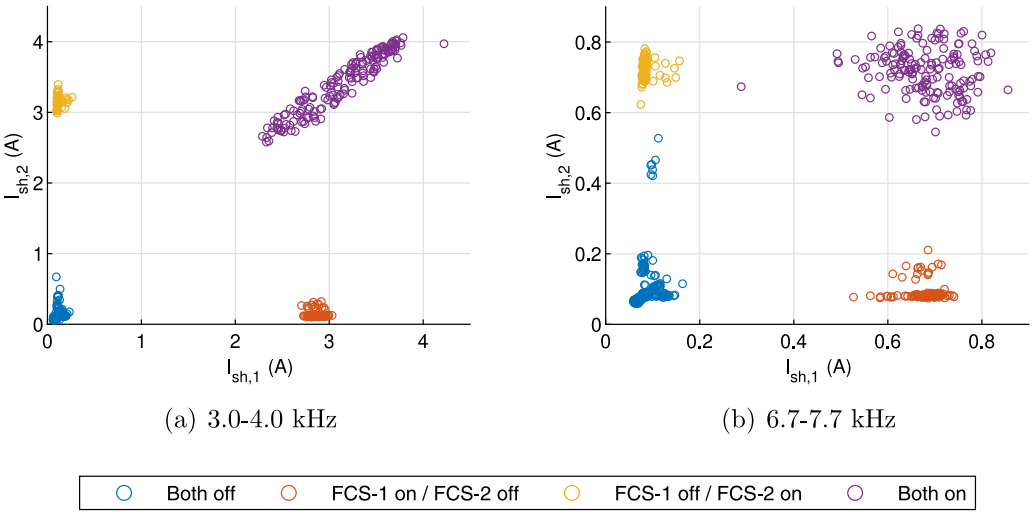

Fig. 4. Secondary emission of FCS-1 and FCS-2, for different on/off states. In this data, FCS-3 and FCS-4 are never active. The chargers absorb emission from each-other, but only when turned on.

result of interaction between the switching frequencies, an amplitude-modulated emission is seen of which the minimum and maximum values can be calculated as described in [14].

Note the difference in primary emission between the chargers, charger 1 ($I_{sh,1}$) has a slightly lower emission than charger 2 ($I_{sh,2}$), this is visible in the combination as well. Also, even for the measurement with both chargers turned off, there is a noise floor in the bins of approximately 100 mA.

4. Results on summation

In this section, an analysis of the SH emission of the installation is presented. The experimental data is clustered in groups based on the number of active chargers (N), as discussed. There are 466 data-points for N = 1, 621 for N = 2, 487 for N = 3 and 69 for N = 4. The emission amplitude of the installation is not constant over time and in this section, the relation between the total emission and the number of active chargers is studied.

The emission is expressed with the 50th (median), 95th and 99th percentiles. Depending on the connection requirements and the type of assessment, either one of the percentiles or the median value is of interest. For the assessment of the thermal impact, the median value gives a better representation in terms of long-term impact, whereas the 95th and 99th percentiles are used for the assessment of short-term or peak behavior that can for instance lead to interaction or interference with other devices.

4.1. 3.0–4.0 kHz

The emission between 3.0 and 4.0 kHz bin in the total current from the installation is presented in Fig. 5 for a different number of chargers active. It is observed that an increasing number of active chargers does result in higher peak emission values but has a limited effect on the median values. The cumulative distribution function (c.d.f.) shows some separation for the states with 2, 3, and 4 chargers active, and the lowest emission is observed for the state with 1 charger active. It should be noted that there are fewer measurement points for the state with 4 chargers active, which may impact the results. The conclusion on the summed emission is dependent on the percentiles considered. Hence, in Table 2 the percentiles of the emission are considered and the same trend is visible. The maximum increase per charger in SH emission is a factor of 1.54 based on the 95th percentiles and 1.51 based on the 99th percentiles. The highest emission is observed for the state with 4 chargers active where the 99th percentile of the emission is 2.17 times

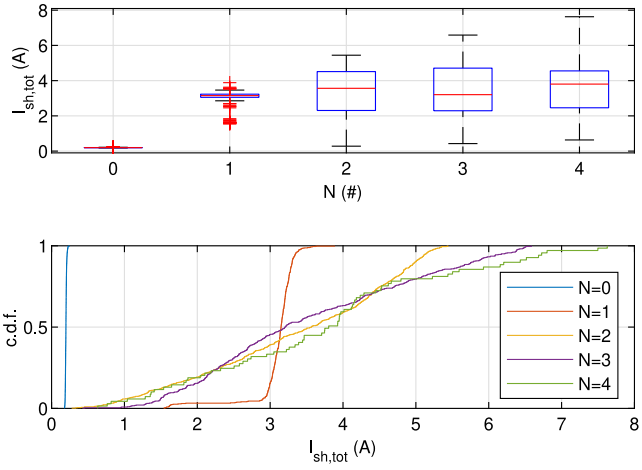

Fig. 5. Emission ($I_{sh,tot}$) between 3.0 and 4.0 kHz from installation for a different amount of chargers active (N). More active chargers increase the peak values but have a limited effect on the median values.

Table 2
Percentiles of SH emission $I_{sh,tot}$ (A) from installation.

N	3.0–4.0 kHz			6.7–7.7 kHz		
	50th	95th	99th	50th	95th	99th
1	3.1	3.3	3.5	0.7	0.8	1.0
2	3.5	5.1	5.3	1.0	1.4	1.5
3	3.2	6.2	6.5	1.2	2.0	2.1
4	3.8	6.7	7.6	1.4	2.5	3.0

higher than the 99th percentile of the emission from a single charger. However, this emission is only 1.08 times higher than the emission for 3 chargers.

4.2. 6.7–7.7 kHz

The supraharmonic emission in the 6.7–7.7 kHz bin is presented in Fig. 6 for a different number of chargers active. It is observed that for an increasing amount of chargers active, the supraharmonic emission in this bin increases. The c.d.f. show the same behavior, for an increased amount of chargers active the total supraharmonic emission from the installation increases too, and a clear separation of the curves is visible,

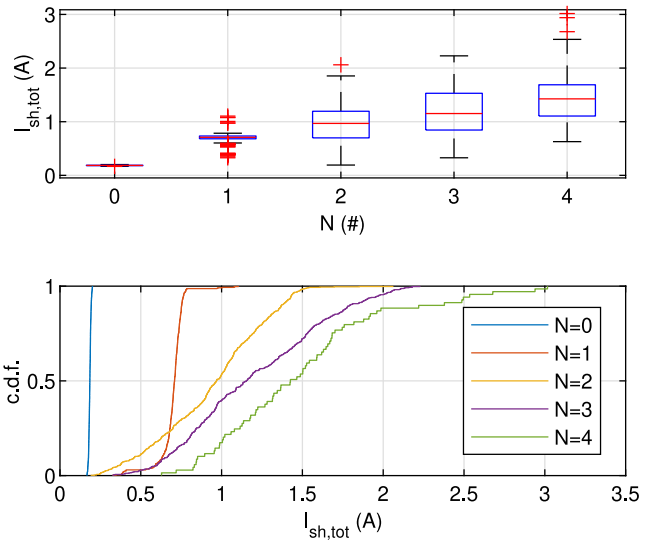

Fig. 6. Emission ($I_{sh,tot}$) between 6.7 and 7.7 kHz from installation for a different amount of chargers active (N). Both the peak and median values increase with the number of active chargers.

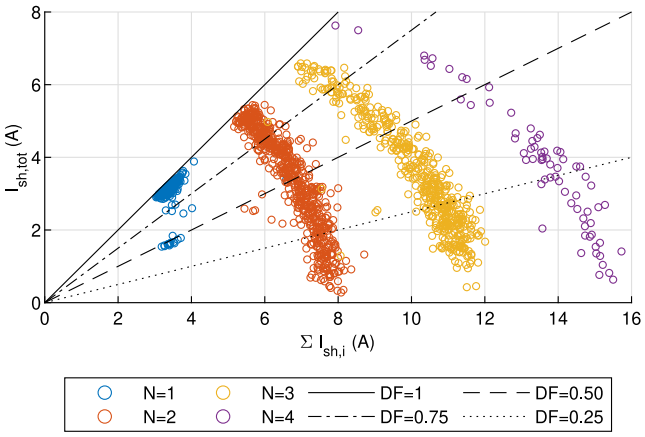

Fig. 7. Relation between total measured current ($I_{sh,tot}$) and the arithmetical sum of individual current $\sum I_{sh,i}$ between 3.0 and 4.0 kHz for a different amount of chargers active (N). Lines with constant diversity factor (DF) included.

compared to the emission between 3.0 and 4.0 kHz. The median values (50th percentile) of the emission increase clearly and the highest peak values are observed for the state with 4 chargers active. Similar findings are observed in the percentiles of the emission, as presented in Table 2. The maximum increase in emission for an extra charger is a factor of 1.75 based on the 95th percentile and 1.50 based on the 99th percentile. The highest emission for the 99th percentile is 3.0 times higher than the emission from a single charger, and 3.13 for the 95th percentile, which is 1.25 times higher than the emission for 3 chargers (95th percentile).

5. Diversity factor

The diversity factor (DF_h) is described by the authors of [35] to quantify the summation of harmonic currents. It is defined as the ratio between the phasor sum of the currents and the arithmetical sum of the currents, resulting in a ratio between 0 and 1 due to diversity in harmonic phase angles from individual devices. The DF_h describes the summation of harmonic currents in an installation. An analogous expression for DF_h, based on the availability of measurement data for the individual and total currents, is defined by [36] as the ratio between the total measured current ($I_{h,tot}$) and the arithmetical sum of measured individual harmonic currents ($\sum I_{h,i}$) where h is the harmonic index and i the device index. Both [35,36] consider the diversity factor for harmonic currents only.

Similar to harmonic currents, supraharmonics currents sum as vectors based on their phase angles, and the diversity factor for supraharmonics is defined as

$$DF_{sh} = \frac{I_{sh,tot}}{\sum I_{sh,i}} \tag{2}$$

with $I_{sh,tot}$ the total measured current in the supraharmonic bin and $\sum I_{sh,i}$ the arithmetical sum of the individual supraharmonic bin currents, based on the expression in [36]. The phase angles can be different between devices and for different frequencies. However, the phase angle of a SH component can be difficult to measure and compare as there is no reference angle and the SH components are mostly unrelated to the fundamental. Furthermore, when using a bin the phase representation as for harmonics no longer holds; there is no angle of a bin and the different components can vary over time. The diversity factor for supraharmonics is not defined for a specific frequency component, but for a bin in which multiple components that are mutually related can be present. In this way, variations in the switching frequency can be covered as long as the variations are within the bin.

5.1. Results for 3.0–4.0 kHz

The relation between the measured total current $I_{sh,tot}$ and the arithmetical sum of the measured individual currents $\sum I_{sh,i}$ of 4 chargers is presented in Fig. 7 for frequencies between 3 and 4 kHz. In the figure, four separate groups of data points are shown, representing the different states of the installation for which one, two, three, or four chargers are active. There are fewer data points for the latter, in line with the observation that only for a limited number of snapshots 4 chargers are active simultaneously. It is observed that for an increasing number of devices active, the peak values for both the total and the summed individual currents increase. However, the summed $\sum I_{sh,i}$ values are in general higher than the total measured current $I_{sh,tot}$ due to the diversity. The summation of the SH currents in this bin is hence not arithmetical.

The percentiles of the diversity factor for different states are shown in Table 3. It is observed that for an increasing number of chargers active the median of the diversity factor decreases. This implies that additional SH sources do not lead to a proportional increase in the total supraharmonic current emitted by the installation, which is in line with the findings in Section 4. The diversity factor is expressed based on different probabilities, the median, 95th, and 99th percentiles. It is concluded that the supraharmonic components in the 3–4 kHz bin do not sum arithmetically and that the DF_{sh} decreases with a higher number of devices.

5.2. Results for 6.7–7.7 kHz

For the 6.7 to 7.7 kHz bin the results are presented in Fig. 8. The diversity factor has different behavior for this frequency band, a decrease in diversity is observed for an increasing number of devices. Also here the increase in peak emission values is observed for a higher number of chargers active and the summed emission is in general higher than the total measured emission. Note that, compared to the 3.0–4.0 kHz bin the current amplitudes are lower and that the data points for 1 charger active do not result in a diversity factor of 1. This is caused by the 100 mA noise floor of the current probes, which results in the summed emission $\sum I_{sh,i}$ to appear higher due to the summation of 3 times the noise level for the idle chargers in the state with 1 charger active. This, in combination with the lower emission amplitude, results in general in lower DF values for this bin.

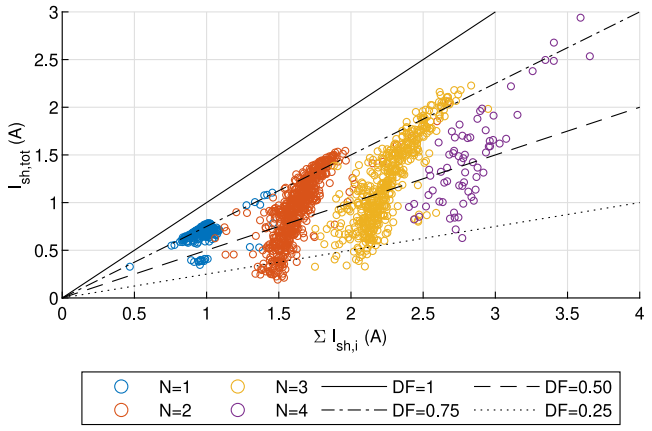

Fig. 8. Relation between total measured current ($I_{sh,tot}$) and the arithmetical sum of individual current $\sum I_{sh,i}$ between 6.7 and 7.7 kHz for a different amount of chargers active (N). Lines with constant diversity factor (DF) included.

Table 3
Diversity factor DF based on 50th, 95th and 99th percentiles.

N	3.0–4.0 kHz			6.7–7.7 kHz		
	DF_{50}	DF_{95}	DF_{99}	DF_{50}	DF_{95}	DF_{99}
1	0.94	0.96	0.96	0.73	0.76	0.76
2	0.53	0.93	0.96	0.60	0.78	0.80
3	0.30	0.82	0.92	0.52	0.76	0.79
4	0.38	0.65	0.95	0.52	0.74	0.82

The numerical values for the diversity factor in the 6.7–7.7 kHz bin are shown in Table 3. The values show the same trend as presented in the figures; for 3.0–4.0 kHz there is a decrease in DF for an increasing number of chargers, and for the 6.7–7.7 kHz the decrease is also present but less significant.

6. Discussion

The emission from the installation shows large variations over time and therefore, the diversity factor cannot be generalized to one single parameter. Also, depending on the number of chargers the summation of SHs is different due to the changing installation impedance as seen by the individual chargers due to the switching of the EMC filters of the chargers as demonstrated in Fig. 4. Future research can consider this effect and determine if the DF will also change in installations where the EMC filters remain connected and study the behavior for higher frequencies than in this research.

6.1. On variations in the total emission

In Section 4 the emission from the installation is discussed. It is observed that the emission cannot be generalized to a single value and that the amplitudes vary across a band. Hence, a time–frequency analysis of the emission spectra is performed using the short-time Fourier transform, obtained using the spectrogram function of MATLAB, with parameters as presented in the figure caption. In Fig. 9(a) the result for the emission between 3.0 and 4.0 kHz of the installation ($I_{sh,tot}$) is shown when only charger 1 is active. The analysis from the previous section used a 200 ms window in line with standardization, whereas each measurement contains 500 ms of data. In the spectrogram, the Fourier transform is calculated with windows of 50 ms, resulting in 10 windows for the measurement length. It is observed that the emission is not varying in amplitude within the measurement window in the case with one charger active.

In Fig. 9(b) the spectrogram of the total current ($I_{sh,tot}$) from the installation for the state with 2 chargers active is presented. It is observed that the emission, in this case, is not constant over time, and that it fluctuates within the measurement window of 500 ms. It is not clear whether the complete period of the fluctuation is visible, but based on the figure it is likely to be at least 500 ms. This explains the variations in total emission when 2 or more chargers are active.

6.2. On impedance

The grid impedance is assumed constant and with a resistive and inductive nature due to the short cable lengths and hence mainly determined by the transformer according to

$$Z_{grid}(f) = R + j2\pi f L \tag{3}$$

with R and L the resistive and inductive components. Based on the transformer specifications as shown in Fig. 1, the upstream impedance of the transformer (at 50 Hz) is calculated as

$$Z_{sc} = U_k \cdot \frac{U_n}{I_n} \tag{4}$$

with U_n and I_n the nominal voltage and current on the secondary side. To estimate the impedance for higher frequencies (f), this value could be linearly multiplied by $f/50$. However, a more accurate result is achieved when only the inductive part of the impedance is scaled with frequency as

$$Z_{est}(f) = |R_{sc} + j \cdot f \cdot \frac{X_{sc}}{50}| \tag{5}$$

with R_{sc} the short-circuit resistance and X_{sc} the short circuit reactance at 50 Hz. Now, a higher X_{sc} will result in a steeper increase of impedance for increasing frequency and, as a result, will decrease the high-frequency currents flowing towards the transformer.

The amplitude of the supraharmonics grid impedance can also be estimated based on the measurement data, using the current injected by the installation into the grid $I_{sh,tot}$, and the resulting voltage disturbance V_{sh} and calculating the ratio according to

$$|Z_{grid}| = \frac{V_{sh}}{I_{sh,tot}} \tag{6}$$

and this gives the result and impedance estimates shown in Fig. 10. The transformer impedance estimates calculated using (5) give slightly different results (0.43 Ω and 0.90 Ω), probably due to the lack of cables and filters in this estimation and the missing resonances due to this. Substituting the measured values for the center frequencies of the bins (3.6 and 7.2 kHz) gives an estimate of the R and L values for the grid, which are 0.35 Ω and 14.9 μH respectively.

In Fig. 11 a part of the data from Fig. 7 is presented for N = 2. The emission forms a curve that cannot be explained by amplitude modulation. For a higher summed emission ($\sum I_{sh,i}$) the total emission towards the grid ($I_{sh,tot}$) is lower, see Region B. Here the same holds for the voltage disturbance V_{sh} and diversity factor DF_{sh}. The grid impedance is constant, hence an explanation for this decrease in total emission is that the impedance of the chargers decreases when their emission is higher. Hence, the filters of the chargers then absorb more emissions. On the other hand, in Region A where the emission is mainly absorbed by the grid, V_{sh} and DF_{sh} are the highest, are the points where the summed emission is lowest. Hence, the chargers impedance is assumed higher in Region A compared to Region B, and as a result, less emission is absorbed by the chargers.

For the 6.7–7.7 kHz bin the curve appears differently, and here the regions with a higher summed emission also result in a higher total emission. It is expected that for this frequency the impedance of the chargers has less influence on the absorption and hence the ratio of the device and grid impedance is higher compared to the 3.0–4.0 kHz band. This is also reflected in higher median values of the DF for the 6.7–7.7 kHz band.

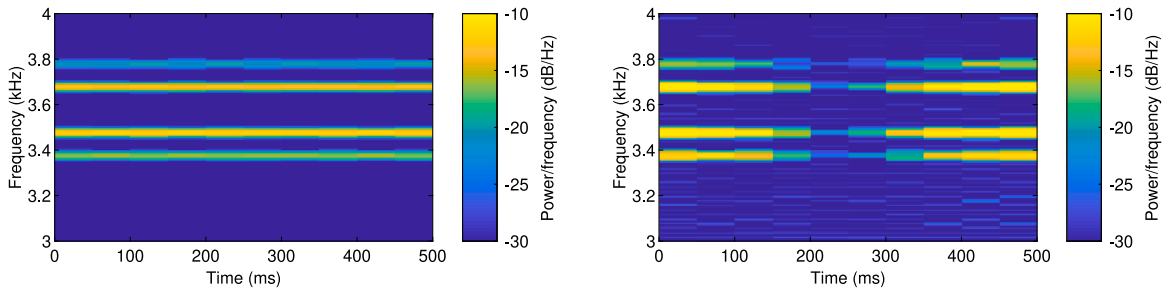

(a) 1 charger active (b) 2 chargers active

Fig. 9. Time–frequency plot of $I_{sh,tot}$ between 3.0–4.0 kHz for 500 ms with 1 or 2 chargers active. Window width of 50 ms, no overlap, 2e5 FFT points (nfft). Obtained using MATLAB's spectrogram function.

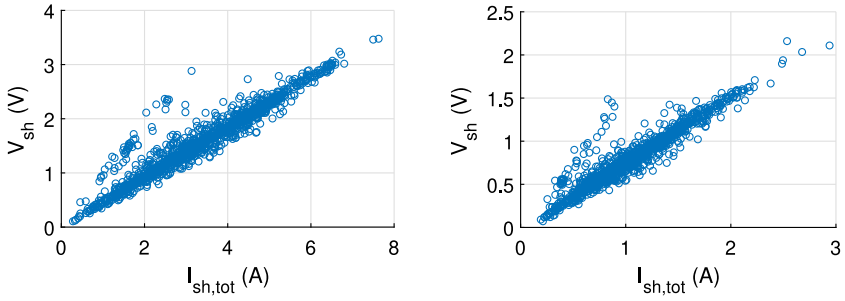

(a) 3.0-4.0 kHz: $|\overline{Z}_{grid}| = 0.48\Omega$ (b) 6.7-7.7 kHz: $|\overline{Z}_{grid}| = 0.76\Omega$

Fig. 10. Relation between V_{sh} and $I_{sh,tot}$, used to estimate the grid impedance for the frequency bins according to (6).

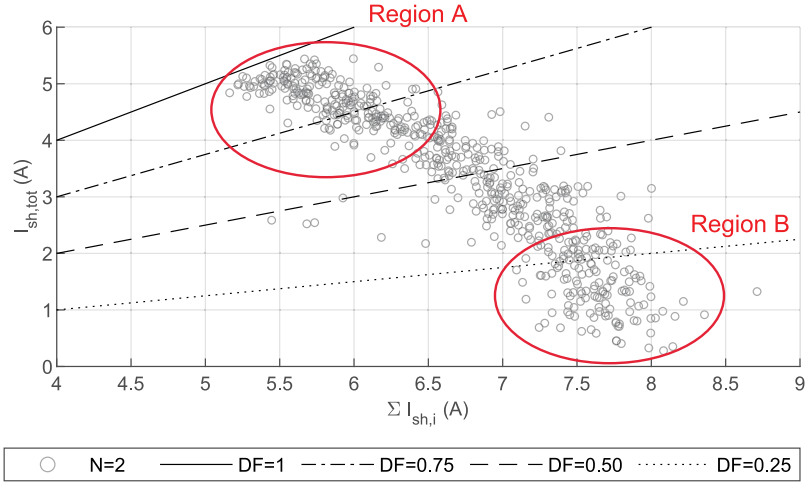

Fig. 11. Part of data from Fig. 7 for N = 2, with indication of regions A and B, which shows different summation effects.

6.3. On variations in emission of a single charger

Findings by the authors of [37] provide insight into variations of the SH emission of a single charger. In this research, the supraharmonic emission of a 175 kW fast-charging station for bus charging is characterized in a controlled lab environment. The output parameters (output power, DC-voltage) of the charger are controlled and the SH emission is characterized for different operating conditions. Here it is found that the SH emission in certain frequency bands is highly sensitive to variations in the DC output voltage of the charger and less sensitive to variations in output power. In this research, the correlation of SH emission with input power did not show a clear relation. However, based on these findings it is likely that some variations in SH emission are due to variations in the output voltage of the chargers.

6.4. On limitations in field measurements

The findings in this research are based on field measurements, to achieve insight into the real impact of installations with FCSs and to see whether existing summation models are representative. The unique behavior of- and interaction between multiple FCSs of considerably large power and a large diversity in types and manufacturers can only be studied in field measurements. Compared to lab measurements, there are some limitations in field measurements. At first, the results from field measurements can be influenced by the background voltage distortions that are present. Secondly, the charging parameters (e.g. charging power, DC-voltage) are not controllable nor measured as they are determined by the EV, which is of interest for future research.

7. Conclusion

In this article, the emission and summation of supraharmonic currents from fast-charging stations are studied. A diversity factor for SHs is proposed and the relation between summed and total current is studied. The findings of this work are summarized as follows:

- The FCSs are a source of SH currents between 3.0–4.0 kHz and 6.7–7.7 kHz.
- When turned on, the FCSs absorb SH currents from the other chargers.
- The SH emission from the installation increases with the number of active chargers with a factor between 1.08 and 1.75 (95th percentile) depending on the number of chargers.
- This increase in emission, however, is not monotonous and slows down for a higher number of active chargers.
- Variations in the total emission are due to interaction between the chargers.
- A higher number of active chargers decreases the diversity factor (e.g. from 0.93 to 0.65 in the 3.0–4.0 kHz bin, for N = 2 and N = 4 respectively, based on the 95th percentile).
- It is likely that the charger impedance is not constant and has an effect on the absorption and hence summation of the emission.

Based on these outcomes, further research is recommended on the summation of SHs for installations with high power. It can focus on locations with an even higher number of chargers and simultaneous charging sessions to study the summation in practice, and, see whether a decrease in emission is visible for a higher number of chargers. Additionally, measurements of the impedance of power-electronic devices in the supraharmonic frequency range are required to study its effect on absorption. Furthermore, it is of interest to study other installations with large power-electronic equipment, like photovoltaic- or battery-storage inverters. It is recommended to use the findings in future modeling of the SH emission and summation.

CRediT authorship contribution statement

Tim Slangen: Conceptualization, Methodology, Software, Formal analysis, Investigation, Writing – original draft. **Vladimir Ćuk:** Conceptualization, Validation, Supervision, Resources, Writing – review & editing. **Sjef Cobben:** Supervision, Writing – review & editing.

Declaration of competing interest

The authors declare the following financial interests/personal relationships which may be considered as potential competing interests: Tim Slangen reports financial support was provided by Topsector Energysubsidy of the Dutch Ministry of Economic Affairs and Climate.

Data availability

The data that has been used is confidential

References

[1] L. Wang, Z. Qin, T. Slangen, P. Bauer, T. van Wijk, Grid impact of electric vehicle fast charging stations: Trends, standards, issues and mitigation measures - an overview, IEEE Open J. Power Electron. 2 (2021) 56–74, http://dx.doi.org/10.1109/OJPEL.2021.3054601.

[2] F. Chen, Q. Zhong, H. Zhang, M. Zhu, S. Müller, J. Meyer, W. Huang, Survey of harmonic and supraharmonic emission of fast charging stations for electric vehicles in China and Germany, in: 26th International Conference on Electricity Distribution (CIRED 2021), Geneva, Switzerland, 2021, p. 5, http://dx.doi.org/10.1049/icp.2021.1927.

[3] T. Slangen, S. Bhattacharyya, Determining the impacts of fast-charging of electric busses on the power quality based on field measurements, in: 26th International Conference on Electricity Distribution (CIRED 2021), Geneva, Switzerland, 2021, p. 5, http://dx.doi.org/10.1049/icp.2021.1989.

[4] S.K. Rönnberg, M.H. Bollen, H. Amaris, G.W. Chang, I.Y. Gu, H. Kocewiak, J. Meyer, M. Olofsson, P.F. Ribeiro, J. Desmet, On waveform distortion in the frequency range of 2 kHz–150 kHz—Review and research challenges, Electr. Power Syst. Res. 150 (2017) 1–10, http://dx.doi.org/10.1016/j.epsr.2017.04.032.

[5] E.O.A. Larsson, M.H.J. Bollen, M.G. Wahlberg, C.M. Lundmark, S.K. Rönnberg, Measurements of high-frequency (2–150 kHz) distortion in low-voltage networks, IEEE Trans. Power Deliv. 25 (3) (2010) 1749–1757, http://dx.doi.org/10.1109/TPWRD.2010.2041371.

[6] Y. Wang, D. Luo, X. Xiao, Evaluation of supraharmonic emission levels of multiple grid-connected VSCs, IET Gener. Transm. Distrib. 13 (24) (2019) 5597–5604, http://dx.doi.org/10.1049/iet-gtd.2019.0182.

[7] R. Torquato, G. Tessmer Hax, W. Freitas, A. Nassif, Impact assessment of high-frequency distortions produced by PV inverters, IEEE Trans. Power Deliv. 36 (5) (2021) 2978–2987, http://dx.doi.org/10.1109/TPWRD.2020.3031375, Conference Name: IEEE Transactions on Power Delivery.

[8] M. Knenicky, R. Prochazka, J. Hlavacek, O. Sefl, Impact of high-frequency voltage distortion emitted by large photovoltaic power plant on medium voltage cable systems, IEEE Trans. Power Deliv. 36 (3) (2021) 1882–1891, http://dx.doi.org/10.1109/TPWRD.2020.3016952.

[9] O. Lennerhag, A. Dernfalk, P. Nygren, Supraharmonics in the presence of static frequency converters feeding a 16 Hz railway system, in: 2020 19th International Conference on Harmonics and Quality of Power (ICHQP), IEEE, Dubai, United Arab Emirates, 2020, pp. 1–6, http://dx.doi.org/10.1109/ICHQP46026.2020.9177901.

[10] S.T.Y. Alfalahi, A.A. Alkahtani, A.Q. Al-Shetwi, A.S. Al-Ogaili, A.A. Abbood, M.B. Mansor, Y. Fazea, Supraharmonics in power grid: Identification, standards, and measurement techniques, IEEE Access 9 (2021) 103677–103690, http://dx.doi.org/10.1109/ACCESS.2021.3099013.

[11] L. Paulsson, B. Ekehov, S. Halen, T. Larsson, L. Palmqvist, A.-A. Edris, D. Kidd, A. Keri, B. Mehraban, High-frequency impacts in a converter-based back-to-back tie; the eagle pass installation, IEEE Trans. Power Deliv. 18 (4) (2003) 1410–1415, http://dx.doi.org/10.1109/TPWRD.2003.817724, Conference Name: IEEE Transactions on Power Delivery.

[12] C. Unger, K. Kruger, M. Sonnenschein, R. Zurowski, Disturbances due to voltage distortion in the khz range-experiences and mitigation measures, in: 18th International Conference and Exhibition on Electricity Distribution (CIRED 2005), Vol. 2005, IEE, Turin, Italy, 2005, pp. v2–23–v2–23, http://dx.doi.org/10.1049/cp:20051018.

[13] S.K. Ronnberg, M. Wahlberg, M.H.J. Bollen, C. Lundmark, Equipment currents in the frequency range 9–95 kHz, measured in a realistic environment, in: 2008 13th International Conference on Harmonics and Quality of Power, 2008, pp. 1–8, http://dx.doi.org/10.1109/ICHQP.2008.4668745, ISSN:2164-0610.

[14] S. Ronnberg, A. Larsson, M. Bollen, J.-L. Schanen, A simple model for interaction between equipement at a frequency of some tens of KHz, in: 21st International Conference on Electricity Distribution, Frankfurt, Germany, 2011, p. 4.

[15] A. Espin-Delgado, S. Ronnberg, T. Busatto, V. Ravindran, M. Bollen, Summation law for supraharmonic currents (2–150 kHz) in low-voltage installations, Electr. Power Syst. Res. 184 (2020) 106325, http://dx.doi.org/10.1016/j.epsr.2020.106325.

[16] M.H.J. Bollen, S.K. Ronnberg, Primary and secondary harmonics emission; harmonic interaction - a set of definitions, in: 2016 17th International Conference on Harmonics and Quality of Power (ICHQP), IEEE, Belo Horizonte, Brazil, 2016, pp. 703–708, http://dx.doi.org/10.1109/ICHQP.2016.7783333.

[17] F. Zavoda, R.R. Puertas, J.-L. Dupré, Impact of fast charging stations on grid quality, in: 25th International Conference on Electricity Distribution (CIRED), Madrid, Spain, 2019, p. 5, http://dx.doi.org/10.34890/378.

[18] J. Meyer, S. Mueller, S. Ungethuem, X. Xiao, A. Collin, S. Djokic, Harmonic and supraharmonic emission of on-board electric vehicle chargers, in: 2016 IEEE PES Transmission & Distribution Conference and Exposition-Latin America (PES T&D-la), Morelia, Mexico, 2016, pp. 1–7, http://dx.doi.org/10.1109/TDC-LA.2016.7805641.

[19] T. Slangen, T.v. Wijk, V. Cuk, J.F.G. Cobben, The harmonic and supraharmonic emission of battery electric vehicles in the netherlands, in: 2020 International Conference on Smart Energy Systems and Technologies (SEST), Istanbul, Turkey, 2020, p. 6, http://dx.doi.org/10.1109/SEST48500.2020.9203533.

[20] D. Darmawardana, J. David, S. Perera, D. Robinson, J. Meyer, U. Jayatunga, Analysis of high frequency (supraharmonics) emissions caused by electric vehicle charging, in: 2020 19th International Conference on Harmonics and Quality of Power (ICHQP), Dubai, United Arab Emirates, 2020, p. 6, http://dx.doi.org/10.1109/ICHQP46026.2020.9177932.

[21] A.J. Collin, S.Z. Djokic, H.F. Thomas, J. Meyer, Modelling of electric vehicle chargers for power system analysis, in: 11th International Conference on Electrical Power Quality and Utilisation, IEEE, Lisbon, Portugal, 2011, pp. 1–6, http://dx.doi.org/10.1109/EPQU.2011.6128816.

[22] X. Xiao, H. Molin, P. Kourtza, A. Collin, G. Harrison, S. Djokic, J. Meyer, S. Muller, F. Moller, Component-based modelling of EV battery chargers, in: 2015 IEEE Eindhoven PowerTech, IEEE, Eindhoven, Netherlands, 2015, pp. 1–6, http://dx.doi.org/10.1109/PTC.2015.7232690.

[23] R. Horton, J.A. Taylor, A. Maitra, J. Halliwell, A time-domain model of a plug-in electric vehicle battery charger, in: PES T&D 2012, Orlando, FL, USA, 2012, pp. 1–5, http://dx.doi.org/10.1109/TDC.2012.6281409.

[24] T. Kirsa, A Norton Approach to Electric Vehicle DC Charger Modelling for Harmonic Studies (M.S. thesis), Dept. of Electrical Energy Systems, Eindhoven University of Technology, Eindhoven, Netherlands, 2020, p. 18.
[25] Y. Sun, E. De Jong, V. Cuk, J. Cobben, Ultra fast charging station harmonic resonance analysis in the dutch MV grid: application of power converter harmonic model, CIRED - Open Access Proc. J. 2017 (1) (2017) 879–882, http://dx.doi.org/10.1049/oap-cired.2017.1074.
[26] S. Cassano, F. Silvestro, E.D. Jaeger, C. Leroi, Modeling of harmonic propagation of fast DC EV charging station in a low voltage network, in: 2019 IEEE Milan PowerTech, Milan, Italy, 2019, p. 6, http://dx.doi.org/10.1109/PTC.2019.8810969.
[27] E. Najafi, A. Vahedi, A. Mahanfar, A.H.M. Yatim, A new controlling method based on peak current mode (PCM) for PFC, in: 2008 IEEE 2nd International Power and Energy Conference, Johor Bahru, Malaysia, 2008, pp. 1103–1107, http://dx.doi.org/10.1109/PECON.2008.4762638.
[28] M. Mythili, N. Kayalvizhi, Harmonic minimization in multilevel inverters using selective harmonic elimination PWM technique, in: 2013 International Conference on Renewable Energy and Sustainable Energy (ICRESE), IEEE, Coimbatore, India, 2013, pp. 70–74, http://dx.doi.org/10.1109/ICRESE.2013.6927790.
[29] S. Schottke, S. Rademacher, J. Meyer, P. Schegner, Transfer characteristic of a MV/LV transformer in the frequency range between 2 kHz and 150 kHz, in: 2015 IEEE International Symposium on Electromagnetic Compatibility (EMC), IEEE, Dresden, Germany, 2015, pp. 114–119, http://dx.doi.org/10.1109/ISEMC.2015.7256142.
[30] S. Sudha Letha, A.E. Delgado, S.K. Ronnberg, M.H.J. Bollen, Evaluation of medium voltage network for propagation of supraharmonics resonance, Energies 14 (4) (2021) 1093, http://dx.doi.org/10.3390/en14041093.
[31] IEC 61000-4-30:2015, Electromagnetic compatibility (EMC) - part 4-30: Testing and measurement techniques - power quality measurement methods, 2015.
[32] IEC 61000-4-7:2002/A1:2009, Electromagnetic compatibility (EMC) - part 4-7: Testing and measurement techniques - general guide on harmonics and interharmonics measurements and instrumentation, for power supply systems and equipment connected thereto, 2009.
[33] D. Ritzmann, S. Lodetti, D. de la Vega, V. Khokhlov, A. Gallarreta, P. Wright, J. Meyer, I. Fernández, D. Klingbeil, Comparison of measurement methods for 2–150-kHz conducted emissions in power networks, IEEE Trans. Instrum. Meas. 70 (2021) 1–10, http://dx.doi.org/10.1109/TIM.2020.3039302.
[34] A. Trzynadlowski, F. Blaabjerg, J. Pedersen, R. Kirlin, S. Legowski, Random pulse width modulation techniques for converter-fed drive systems-a review, IEEE Trans. Ind. Appl. 30 (5) (1994) 1166–1175, http://dx.doi.org/10.1109/28.315226.
[35] A. Mansoor, W. Grady, A. Chowdhury, M. Samotyi, An investigation of harmonics attenuation and diversity among distributed single-phase power electronic loads, in: Proceedings of IEEE/PES Transmission and Distribution Conference, 1994, pp. 110–116, http://dx.doi.org/10.1109/TDC.1994.328369.
[36] V. Cuk, J.F. Cobben, W.L. Kling, P.F. Ribeiro, Analysis of harmonic current summation based on field measurements, IET Gener. Transm. Distrib. 7 (12) (2013) 1391–1400, http://dx.doi.org/10.1049/iet-gtd.2012.0620.
[37] T.M.H. Slangen, V. Cuk, J. Cobben, E. de Jong, Variations in supraharmonic emission (2-150 khz) of an EV fast charging station under different supply- and operating conditions, in: 2023 IEEE Power & Energy Society General Meeting (GM), Orlando, Florida, 2023, p. 5, in press.